

JGR Atmospheres

RESEARCH ARTICLE

10.1029/2021JD034651

Key Points:

- Large spatial variability in gaseous oxidized mercury over different land surface types was observed in the Southern Ocean
- Low gaseous oxidized mercury content in the sea-ice region would be to some extent attributed to its greater uptake by sea salt aerosols
- The seasonal melting of first-year sea ice can cause a clear decrease in gaseous oxidized mercury levels

Supporting Information:

Supporting Information may be found in the online version of this article.

Correspondence to:

Z. Xie,
zqxie@ustc.edu.cn

Citation:

Yue, F., Xie, Z., Yan, J., Zhang, Y., & Jiang, B. (2021). Spatial distribution of atmospheric mercury species in the Southern Ocean. *Journal of Geophysical Research: Atmospheres*, 126, e2021JD034651. <https://doi.org/10.1029/2021JD034651>

Received 24 JAN 2021

Accepted 13 AUG 2021

Author Contributions:

Conceptualization: Zhouqing Xie
Funding acquisition: Zhouqing Xie
Investigation: Fange Yue, Zhouqing Xie, Yanxu Zhang
Methodology: Fange Yue, Bei Jiang
Project Administration: Zhouqing Xie
Resources: Jinpei Yan
Supervision: Zhouqing Xie
Visualization: Fange Yue
Writing – original draft: Fange Yue
Writing – review & editing: Fange Yue, Yanxu Zhang

Spatial Distribution of Atmospheric Mercury Species in the Southern Ocean

Fange Yue¹, Zhouqing Xie^{1,2} , Jinpei Yan³ , Yanxu Zhang⁴ , and Bei Jiang¹ 

¹Department of Environmental Science and Engineering, Institute of Polar Environment & Anhui Key Laboratory of Polar Environment and Global Change, University of Science and Technology of China, Hefei, China, ²Center for Excellence in Urban Atmospheric Environment, Institute of Urban Environment, Chinese Academy of Sciences, Xiamen, China, ³Key Laboratory of Global Change and Marine-Atmospheric Chemistry & Third Institute of Oceanography, Ministry of Natural Resource, Xiamen, China, ⁴School of Atmospheric Sciences, Nanjing University, Nanjing, China

Abstract Antarctica and the surrounding Southern Ocean act as an important sink in the global mercury cycle; however, corresponding studies of atmospheric mercury species in these regions are still scarce. Here, we report large-scale observations of atmospheric gaseous elemental mercury (GEM) and gaseous oxidized mercury (GOM) in the Antarctic marine boundary layer (MBL) taken during a summer cruise. There is large variability in the spatial distribution of GOM, which is likely attributable to the diverse land surface types, including coastal Antarctica, sea-ice region, and oceanic region, along the cruise route. In coastal Antarctica, the highest GOM level ($56.23 \pm 47.74 \text{ pg}\cdot\text{m}^{-3}$) might be attributed to the significant in-situ oxidation there. Significant in-situ oxidation of GEM could also occur in the sea-ice region, causing the significant increase of GOM (up to $87.01 \text{ pg}\cdot\text{m}^{-3}$), while the uptake of the high content of sea-salt aerosols in sea-ice regions might efficiently eliminate GOM in the air, resulting in generally lower content of GOM ($13.10 \pm 14.48 \text{ pg}\cdot\text{m}^{-3}$) in the sea-ice region. In the oceanic region, the lowest level of GOM ($3.95 \pm 4.69 \text{ pg}\cdot\text{m}^{-3}$) is due to both the uptake of sea-salt aerosols and the seasonal melting of first-year sea-ice. This study provides insight to understand the mechanisms of the atmospheric mercury cycle in various land surface types in the Antarctic MBL.

1. Introduction

Since the signature of the Minamata Convention, an international convention aimed at controlling Hg emissions on a global scale, on January 19, 2013, environmental Hg contamination has attracted increasing public attention (Angot, Dastoor et al., 2016). Atmospheric Hg has three major forms based on its physical and chemical properties: gaseous elemental mercury (GEM or Hg(0)), gaseous oxidized mercury (GOM), and particle-bound mercury (PBM). GEM, the dominant form that makes up more than 90% of its total content in the surface air, can be transported worldwide owing to its long lifetime in the air (from months up to 1 year) (Horowitz et al., 2017; Radke et al., 2007). GOM and PBM, which can be formed through the oxidation of GEM, are highly reactive, water-soluble, and can be eliminated from the air effectively via dry and wet deposition (Driscoll et al., 2013; Radke et al., 2007).

The polar region plays a unique role in the global Hg cycle due to its particular geographical and weather conditions (Durnford & Dastoor, 2011). Springtime atmospheric mercury depletion events (AMDEs), phenomena in which GEM is significantly depleted to below the detection limit accompanied by a concurrent depletion of ozone (O₃) (Steffen et al., 2008), were first observed in the Arctic in 1995 (Schroeder et al., 1998), and have since then been regularly observed in both polar regions of the Earth (Ebinghaus et al., 2002; Steffen et al., 2008). This highlighted the role of halogen radicals in GEM oxidation in spring and changed our understanding of the Hg cycle (S. Wang et al., 2019; Xie et al., 2008). Although the Arctic has been extensively monitored, studies in the Antarctic region remain rather scarce (Angot, Magand et al., 2016). Several summertime observations of atmospheric Hg have been conducted at a few Antarctic research stations, including the Italian Antarctic Station (74°41'S, 164°07'E) (Sprovieri et al., 2002), Neumayer Station (70°39'S, 8°15'W) (Temme et al., 2003), McMurdo Station (77.86°S, 166.64°E) (Brooks et al., 2008b), and the South Pole (90°S) (Brooks et al., 2008a). J. Wang et al. (2016) reported the spatial and diurnal variations of total gaseous mercury (GEM + GOM) along a transect from coastal to central Antarctica. These

observations revealed that the atmosphere of the Antarctic continent during the sunlit season has a high oxidation capacity that could result in a high GOM content and/or obvious depletion of GEM (Angot, Dastoor et al., 2016). Several studies have shown that the Antarctic Plateau plays a key role in influencing the atmospheric Hg cycle at a continental scale (Angot, Dastoor et al., 2016; Li et al., 2020; Temme et al., 2003).

Antarctic marine ecosystems are sensitive to the bioaccumulation of Hg, while there are still gaps in our understanding of the mechanisms of the Hg cycle in the Antarctic MBL. Elevated concentrations of Hg have been observed in seawater near Antarctica (Cossa et al., 2011; Nerentorp Mastromonaco, Gårdfeldt, Assmann, et al., 2017; Wang et al., 2017), and even contamination in Antarctic biota have been found (Bargagli, 2008; Brasso et al., 2012; Carravieri et al., 2014). Atmospheric deposition is a principal pathway for Hg to enter the ocean (Soerensen et al., 2010; Steve et al., 2007), mainly in the form of oxidized mercury (e.g., GOM or PBM). The constituents of deposited inorganic mercury would be converted into more toxic organometallic forms (e.g., CH₃Hg) followed by bioaccumulation and biomagnification in Antarctic marine food webs (M. G. Nerentorp Mastromonaco et al., 2016). However, records of Hg concentration in the Antarctic MBL have been sparse to date. Moreover, in most cases, only GEM (or total gaseous mercury) has been measured among atmospheric Hg species (Soerensen et al., 2010; Xia et al., 2010). The lack of observations of oxidized Hg restricts our understanding of the mechanisms of the Hg cycle and our evaluations of atmospheric Hg deposition in the Antarctic MBL. In addition, the presence of sea-ice, which is unique to polar seas, also plays a special role in the regional Hg cycle. Sea-ice both affects the sea-air exchange of Hg and provides a reaction interface for the photochemical transformation thereof (Chaulk et al., 2011; Nerentorp Mastromonaco, Gårdfeldt, & Langer, 2017). Both enhanced GEM and dissolved gaseous mercury (DGM) concentrations have been found in sea-ice covered areas (Wang et al., 2017). It is widely believed that the annual sea-ice area during polar springtime is an important source of atmospheric halogen radicals, leading to the oxidation and subsequent deposition of GEM. Several previous observations have shown that the atmospheric oxidized Hg in the sea-ice area mainly takes the form of PBM (M. Nerentorp Mastromonaco et al., 2016; Steffen et al., 2013); this is different from the characteristics of the Hg species in polar coastal and inland areas, where there usually be a higher GOM presence compared to PBM in Antarctic summertime (Brooks et al., 2008a, 2008b; Temme et al., 2003), and will influence the deposition flux of mercury. However, the mechanism of this phenomenon needs to be explored further.

As part of the 34th Chinese National Antarctic Research Expedition aboard the icebreaker R/V Xuelong, we here report the observations of atmospheric Hg species (GEM, GOM) from areas of open ocean and those covered with sea-ice to the Antarctic coast, as recorded during a large-scale cruise, to investigate the characteristics and corresponding major influence factors of different atmospheric Hg species in various land surface types, therefore facilitate a better understanding of the atmospheric Hg cycle mechanisms in the Antarctic MBL.

2. Materials and Methods

2.1. Study Site

Atmospheric Hg species were measured continuously from Christchurch, New Zealand to eastern and western Antarctica during summer, from November 27, 2017 to April 3, 2018 (Figure 1). Our study sites were generally located in four regions: the southern Pacific Ocean, Ross Sea, Indian sector of Southern Ocean, and the Amundsen Sea. These regional distinctions are for the purpose of data interpretation only and do not necessarily comply with geographical conventions. Further details are provided in Table S1.

2.2. Measurements of Atmospheric Mercury

Continuous measurements of GEM and GOM were conducted using an automated Hg speciation system consisting of a 2537B cold vapor atomic fluorescence spectroscopic Hg analyzer and an 1.130 GOM unit (both from Tekran Inc., Toronto, Canada). GOM was operationally defined as the fraction of oxidized mercury collected on a KCl-coated annular quartz denuder. This system was configured to measure GEM and GOM with a temporal resolution of 5 min and 2 h, respectively. Details on the Tekran Hg speciation system

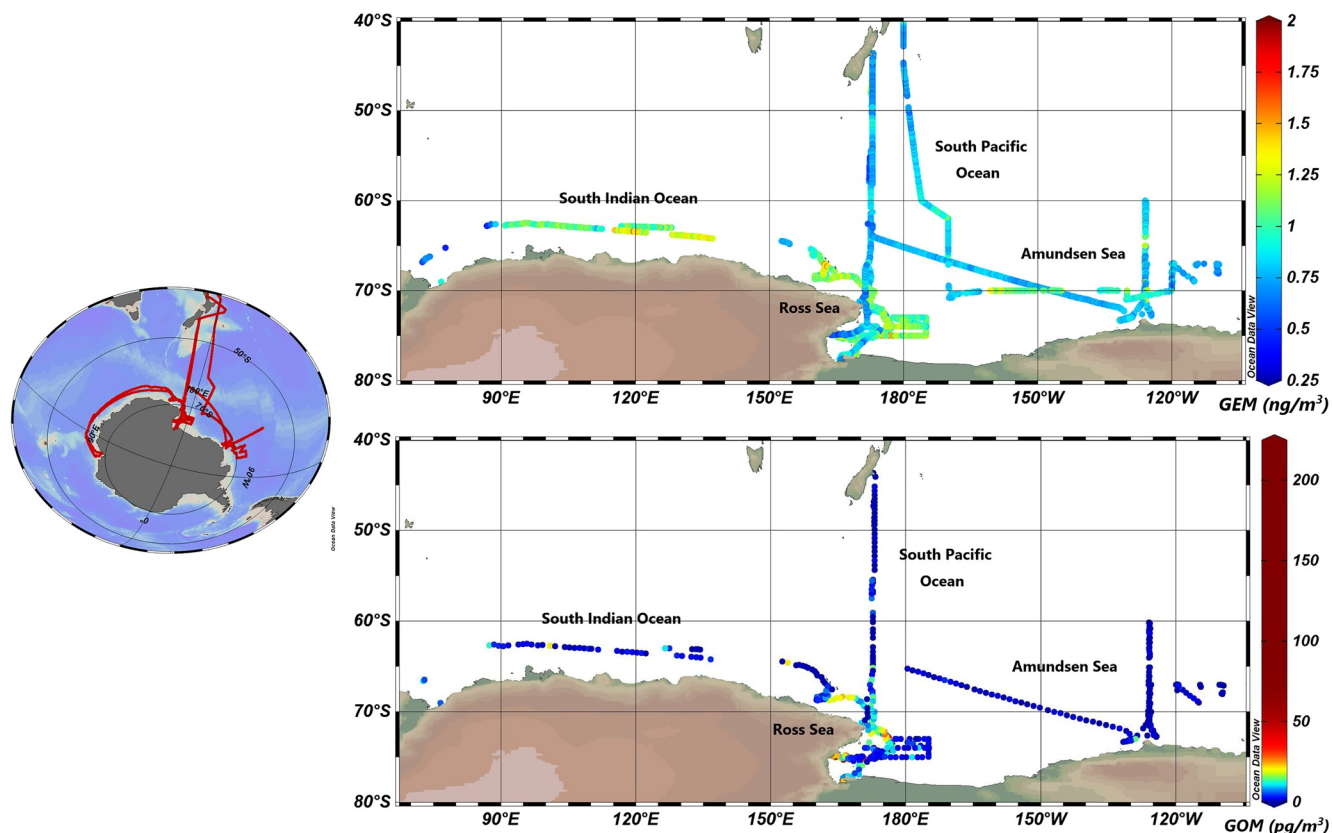


Figure 1. Overviews of (a) gaseous elemental mercury (GEM) and (b) gaseous oxidized mercury (GOM) in the marine boundary layer along these cruise paths (the 34th Chinese National Antarctic Research Expedition); GOM data below instrument detection limits are also displayed. The base map was generated using the software Ocean Data View 4.0.

can be found elsewhere (Landis et al., 2002). The GEM and GOM sampling flow rates were set to 1 and 7 L·min⁻¹, respectively. Coarse particles larger than 2.5 μm were removed at the inlet by a heated impactor.

This Tekran system was placed on the compass deck approximately 35 m above the surface of the sea. The 1,130 unit, which contained the air inlet, was fixed windward at the front of the compass deck and kept away from the power system of the ship to minimize the impact of the plumes emitted from the chimney. The detection limit (DL) for GEM measured by the 2537B unit was better than 0.10 ng·m⁻³. The DL for GOM was estimated to be better than 0.89 pg·m⁻³ based on the sampling volumes. The GEM measurements were calibrated daily via a built-in internal mercury permeation source within the 2537B unit. External calibration using a Tekran 2,505 unit, with manual injections of known concentrations of GEM, was performed before and after the cruise, and the accuracy of both measurements was better than 95%. There are no calibration standards available for GOM, but its 1σ precision is approximately 15% (Landis et al., 2002). To avoid the impact of moisture, two drying tubes containing soda lime were replaced every 4 days. The KCl-coated denuder of the 1,130 unit and Teflon filters (with a pore size 0.2 μm) at the air inlets of the 2537B unit was changed biweekly. Some data loss occurred due to occasional instrument failure, power loss, and ship motions. Other QA/QC procedures followed typical protocols used in similar studies (M. Nerentorp Mastromonaco et al., 2016; Wang et al., 2014).

The Tekran system has been widely used to measure atmospheric Hg speciation (e.g., the Atmospheric Mercury Network (AMNet) of the USA (Gay et al., 2013), the Global Mercury Observation System (GMOS) of the European Union (Sprovieri et al., 2016), and the several Arctic and Antarctic research stations (Domergue et al., 2010; Steffen et al., 2015)); however, previous studies pointed out that the KCl-coated denuder in the Tekran technique cannot efficiently collect all GOM compounds and thus results in an underestimation of GOM (Gustin et al., 2013; Huang & Gustin, 2015). As Gustin's group suggested, one potential

mechanism of the underestimation of GOM by the Tekran system is likely attributed to the presence of moisture and ozone in ambient air, which may cause the reduction of captured GOM to GEM in KCl-coated denuder (Gustin et al., 2013; Huang & Gustin, 2015; McClure et al., 2014). We estimate the effects of humidity and ozone variations on the GOM observations based on McClure et al. (2014) (see details in the supplementary information). It generally displays that when the latitude was within the range of 60°S–80°S, the O₃ and absolute humidity (AH) levels were both low, with a small variation range, which could lead to high recovery of GOM (closed to 1); when the latitude was within the range of 45°S–60°S, the high AH level might lead to larger uncertainty of GOM, but the GOM level in this latitude range was very low and the corresponding data amount only accounted for lower than 3% in this study, which would not affect the conclusion significantly either (Figure S1). Besides, another new method to correct the bias of the Tekran GOM observation technique was proposed recently, which suggested that the GOM loss can be corrected by including Hg content detected during the Tekran instrument's flush cycles (Maruszczak et al., 2017). We also evaluated our GOM observed results based on this method and found that the bias in our observations appeared to be negligible (see details in the supplementary information). In fact, Gustin's recent review paper also suggested that "We expect that KCl-denuder derived data is best for polar regions or high elevation locations in the free troposphere for these areas are dominated by halogenated compounds and dry air" in Section 6 of this paper (Gustin et al., 2021). In summary, we think that the uncertainty of GOM measurement from the Tekran system may not fundamentally change our main discussion and conclusions in this study based on our evaluations of GOM data, and we caution that the GOM results reported in this study should be considered as the lower limits of atmospheric GOM (Wang et al., 2014).

2.3. Other Ancillary Data and Analysis

Ozone was continuously measured using ultraviolet photometry (49i; Thermo Fisher, Inc., USA) at a temporal resolution of 1 min. Its air inlet, which was equipped with Teflon filters (pore size 0.2 μm) to remove coarse particles, was installed windward of and close to the Hg speciation system inlet. The DL of the 49i unit is 1 part per billion by volume (ppbv). The zero and potential shifts of the instrument were regularly controlled via an internal ozone generator. Nitrous oxides (NO_x) were continuously measured by a chemiluminescence NO-NO₂-NO_x analyzer (42i; Thermo Fisher, Inc., USA). We served NO_x data as an indicator of ship emissions, in view of the high detection limit of Model 42i (0.4ppbvppbv) which may be unsuitable in MBL observation (with background concentration of pptv magnitude) (Carsey et al., 1997; Heikes et al., 1996), and considerable emission of NO_x by ship (Huszar et al., 2009; Vinken et al., 2014). However, according to statistics, the concentration of 85.5% of the NO_x data during this whole cruise was between 0 and 1 ppbv (indicating the baseline fluctuation of the NO_x instrument in view of ship swing during the voyage), which indicated that ship emissions would be minor in most observation periods in this study.

Some of the meteorological data, including wind direction, wind speed, relative humidity (RH), and atmospheric temperature were obtained from shipboard monitoring systems. Data on shortwave radiation (Radiation), sea-ice fraction, and planetary boundary layer height (PBLH) were extracted from the assimilated hourly meteorological data from Goddard Earth Observing System—forward processing (GEOS-FP) meteorological field product (horizontal resolution: 2° × 2.5°). Maps of the density distribution of the BrO· vertical column were generated from Global Ozone Monitoring Experiment-2 (GOME-2) satellite data using the DOAS algorithm (http://www.iup.uni-bremen.de/does/scia_data_browser.htm). The BrO· images can generally display the variations in the boundary layer with a more or less constant offset owing to the relatively constant nature of stratospheric BrO· with few spatiotemporal variations (Lindberg et al., 2002). Hourly aerosol water-soluble Na⁺ concentrations were measured by a semi-continuous in-situ gas and aerosol composition (IGAC) monitoring system performed by the *Third Institute of Oceanography, Ministry of Natural Resources* during this cruise (Yan et al., 2020). Fine particles were enlarged via vapor condensation, accelerated by a conical-shaped impaction nozzle, and collected on an impaction plate, and then analyzed for Na⁺ and other ions via an online ion chromatography system (Dionex ICS-3000, place of manufacture).

The online Hybrid Single Particle Lagrangian Integrated Trajectory (HYSPPLIT) transport and dispersion model from the NOAA-Air Resources Laboratory (<https://www.ready.noaa.gov/hypub-bin/trajtype.pl?runtype=archive>) was used to identify the source of air masses from selected locations.

Table 1

Statistics for 2h-Averaged Gaseous Elemental Mercury (GEM), Gaseous Oxidized Mercury (GOM), and GOM/GEM Ratios (%) in the Three Areas Studied

Regions	2h-averaged GEM (ng/m ³)			GOM (pg/m ³)			GOM/GEM (%)			n
	Range	Average	Median	Range	Average	Median	Range	Average	Median	
Coastal Antarctica	0.54–1.47	0.93 ± 0.24	0.90	4.80–201.23	56.23 ± 47.74	44.09	0.46–23.92	6.51 ± 5.57	4.88	101
Sea-ice region	0.49–1.37	0.99 ± 0.17	1.01	1.03–87.01	13.1 ± 14.48	9.06	0.094–17.31	1.6 ± 2.61	0.93	142
Oceanic region	0.43–1.79	0.92 ± 0.24	0.90	0.90–27.42	3.95 ± 4.69	2.21	0.080–3.37	0.47 ± 0.61	0.23	164

3. Results and Discussion

3.1. Concentrations of Gaseous Elemental Mercury (GEM)

Detailed data including the regional distributions of the measured GEM and GOM are shown in Table S2 and Figure 1, respectively. The lowest GEM concentrations were observed in the southern Pacific Ocean (average: $0.78 \pm 0.15 \text{ ng}\cdot\text{m}^{-3}$, median: $0.76 \text{ ng}\cdot\text{m}^{-3}$, $n = 3,851$). As the existence of the prevailing westerlies accompanied by few distributions of anthropogenic sources in this area, this was likely caused by the dilution of GEM through the strong wind with an average wind speed of 11.42 ms^{-1} , which was the highest recorded during the entire cruise. The regional distribution of GEM in the Antarctic MBL exhibited the following trend: Indian sector of Southern Ocean ($1.08 \pm 0.24 \text{ ng}\cdot\text{m}^{-3}$, $n = 615$) > Ross Sea ($0.96 \pm 0.21 \text{ ng}\cdot\text{m}^{-3}$, $n = 5,683$) > Amundsen Sea ($0.85 \pm 0.18 \text{ ng}\cdot\text{m}^{-3}$, $n = 3,787$) ($p < 0.001$). The GEM levels we observed in the Antarctic region are similar to those reported in the Weddell Sea during spring and at the McMurdo and Neumayer stations in Terra Nova Bay during summer ($0.9\text{--}1.2 \text{ ng}\cdot\text{m}^{-3}$) (Brooks et al., 2008b; M. Nerentorp Mastromonaco et al., 2016; Sprovieri et al., 2002; Temme et al., 2003) (Table S2), but lower than the cruise-based observations of Soerensen et al. (2010) from the western Antarctic ocean ($1.30 \pm 0.16 \text{ ng}\cdot\text{m}^{-3}$) and near the Antarctic Peninsula ($1.55 \pm 0.38 \text{ ng}\cdot\text{m}^{-3}$). These discrepancies reflect the spatiotemporal variability of GEM in the Antarctic MBL. Our results for the GEM concentration in the Antarctic region are apparently lower than those observed in the Arctic region during summertime (e.g., Alert [$1.80 \pm 0.35 \text{ ng}\cdot\text{m}^{-3}$], Barrow [$1.40 \pm 0.27 \text{ ng}\cdot\text{m}^{-3}$]) (Steffen et al., 2015). It would to some extent reflect the more impact of anthropogenic emissions on the atmospheric GEM content in the Arctic region, which is closer to human residences, than Antarctica.

3.2. Concentrations of Gaseous Oxidized Mercury (GOM)

The GOM concentrations observed during this cruise presented a wide range of variations, from lower than the DL to a maximum of $201.22 \text{ pg}\cdot\text{m}^{-3}$. As shown in Table S2 and Figure 1, the average GOM concentrations in the Ross Sea ($23.95 \pm 36.59 \text{ pg}\cdot\text{m}^{-3}$, $n = 309$) and Indian sector of the Southern Ocean ($16.38 \pm 17.99 \text{ pg}\cdot\text{m}^{-3}$, $n = 61$) were several times higher than those in the Amundsen Sea ($2.09 \pm 2.35 \text{ pg}\cdot\text{m}^{-3}$, $n = 34$) and southern Pacific Ocean ($3.89 \pm 3.86 \text{ pg}\cdot\text{m}^{-3}$, $n = 27$). The high spatial differences in the GOM content imply that some special factors efficiently influence the state of the oxidation of atmospheric Hg, causing large variations in GOM concentrations; this will be discussed in more detail below. Moreover, 78% and 54% of the GOM observations in the Amundsen Sea and the southern Pacific Ocean, respectively, were lower than the DL of the instrument. Therefore, the statistical means of the GOM levels shown in Table S2 might, to some extent, overestimate the overall values of the GOM concentrations in these areas as GOM results below the DL were not counted.

The average concentrations of GOM observed in all Antarctic MBL regions during this cruise, and in some previous observations conducted in the Antarctic marginal sea (e.g., the southern Pacific Ocean, southern Atlantic Ocean, and Weddell Sea, Table 1), are largely lower than those observed at several inland Antarctic stations, for example, McMurdo and Terra Nova Bay, which recorded levels of $116 \pm 45 \text{ pg}\cdot\text{m}^{-3}$ and $116.3 \pm 77.8 \text{ pg}\cdot\text{m}^{-3}$, respectively (Brooks et al., 2008b; Sprovieri et al., 2002), and near the Antarctic peninsula ($43 \pm 39 \text{ pg}\cdot\text{m}^{-3}$) during the cruise undertaken by Soerensen et al. (2010). Cruise observations of Hg species near western Antarctica, conducted by Temme et al. (2003) also found that GOM concentrations rose correspondingly as they approached the Antarctic continent. This phenomenon implies different atmospheric Hg cycles over the different land surface types in Antarctica.

To allow clear discussion of the characteristics and mechanisms influencing the spatial distributions of Hg in different land surface types during this cruise, we used Land–Water–Ice indices (LWI), which was extracted from the GEOS-FP (horizontal resolution: $2^\circ \times 2.5^\circ$) hourly meteorological data and derived from the ocean, land, and sea-ice fractions in each grid box, to divide our observation area into three regions: (a) coastal Antarctica (LWI = 1), with the land fraction in each grid box ranges from 50.6% to 92.4%, (b) sea-ice regions (LWI = 2), with the sea-ice fraction in each grid box ranges from 45.7% to 90.2%, and (c) oceanic regions (LWI = 0), with the ocean fraction in each grid box ranges from 63.4% to 100% in this study. Time series for the GEM, GOM, sea-ice fraction, and the corresponding LWI over the duration of this cruise are given in Figure S4.

3.3. Characteristics of Mercury in Different Regions

3.3.1. Overview of the Characteristics of Gaseous Mercury Species

The value series and corresponding spatial distributions of measured GOM are shown for the tree types of regions in this cruise in Figure S5. Also shown are the calculated GOM/GEM (%) ratios, which imply the oxidation degree of gaseous mercury based on the chemistry that leads to AMDEs occurs in the gas phase through oxidation of GEM to GOM (Steffen et al., 2013). The statistics (range, mean, standard deviation, and median) of these measurements are shown in Table 1. Despite sea-ice acting as a barrier to the air-sea exchange (DiMento et al., 2019), the average concentration of GEM in the sea-ice region ($0.99 \pm 0.17 \text{ ng}\cdot\text{m}^{-3}$) is higher than coastal Antarctica ($0.93 \pm 0.24 \text{ ng}\cdot\text{m}^{-3}$, $p < 0.001$) and the oceanic region ($0.92 \pm 0.24 \text{ ng}\cdot\text{m}^{-3}$, $p < 0.001$), respectively. A similar phenomenon was reported by Wang et al. (2017) which observed increased GEM concentrations in the Ross Sea, accompanied by elevated concentrations of DGM in surface seawater and enhanced sea-ice concentrations in nearby regions during the Antarctic summer. The increased GEM observed in the sea-ice region is likely attributed to the accumulation-to-emission effect of DGM from sea-ice lead and the photoreduction of divalent Hg (Hg(II)) among snow and sea-ice surface during Antarctic summertime. In springtime, the Antarctic sea-ice region would be served as a sink of Hg due to the significant Hg deposition through AMDEs. The leaching supplement of Hg from the sea-ice, followed by the photoreduction and bioreduction, would cause the accumulation of DGM among the surface water under the sea-ice, which has obviously higher concentrations than the open seawater (DiMento et al., 2019; M.G. Nerentorp Mastro Monaco et al., 2016; Wang et al., 2017); while in the summertime, sea-ice melt and icebreaking activity of a ship would drive the intensive evasion of these accumulated DGM from the sea-ice leads (Andersson et al., 2008), and the shallow convection driven by the temperature difference between the water in the sea-ice leads and the ambient air, would be conducive to the outgassing of Hg(0) from the leads (McElroy et al., 1999; Moore et al., 2014). Moreover, exposure to sunlight during the polar day would facilitate the photoreduction and release of Hg(II) from the snowpack on the surface of sea-ice. These two factors might co-contribute to the increase of GEM among sea-ice region in the Antarctic summertime (Lalonde et al., 2002; M. Nerentorp Mastro Monaco et al., 2016; Wang et al., 2017). Based on our observations, we inferred that the barrier effect of sea-ice cover on the air-sea exchange of Hg might be changed and/or offset by the evasion of GEM from widespread sea-ice leads and the photoreduction of Hg(II) on the surface of the sea-ice during the Antarctic sunlit season.

Figure S5d shows that, notably, the variabilities of the GOM concentrations and GOM/GEM ratios in coastal Antarctica are clearly larger than those in the sea-ice and ocean regions. There are also significant differences in the average GOM concentrations and GOM/GEM (%) ratios in the three study regions, with the results of coastal Antarctica ($56.23 \pm 47.74 \text{ pg}\cdot\text{m}^{-3}$, 6.51 ± 5.57 , $n = 101$) > sea-ice region ($13.10 \pm 14.48 \text{ pg}\cdot\text{m}^{-3}$, 1.6 ± 2.61 , $n = 142$) > oceanic region ($3.95 \pm 4.69 \text{ pg}\cdot\text{m}^{-3}$, 0.47 ± 0.61 , $n = 164$) ($p < 0.001$) (Table 1). These features further confirm that various land surface types would significantly affect the concentration of oxidized mercury species in the Antarctic MBL. Details of the mechanisms influencing the cycle of gaseous Hg species in each region are discussed in the following sections.

3.3.2. Coastal Antarctica

The highest concentrations of GOM and largest fluctuations thereof measured during this cruise were recorded in coastal Antarctica, with a range of 4.80–201.23 $\text{pg}\cdot\text{m}^{-3}$ (Figure 2a and Table 1). As observations of mercury species were mainly conducted during berthing period in Coastal Antarctica, we firstly estimated

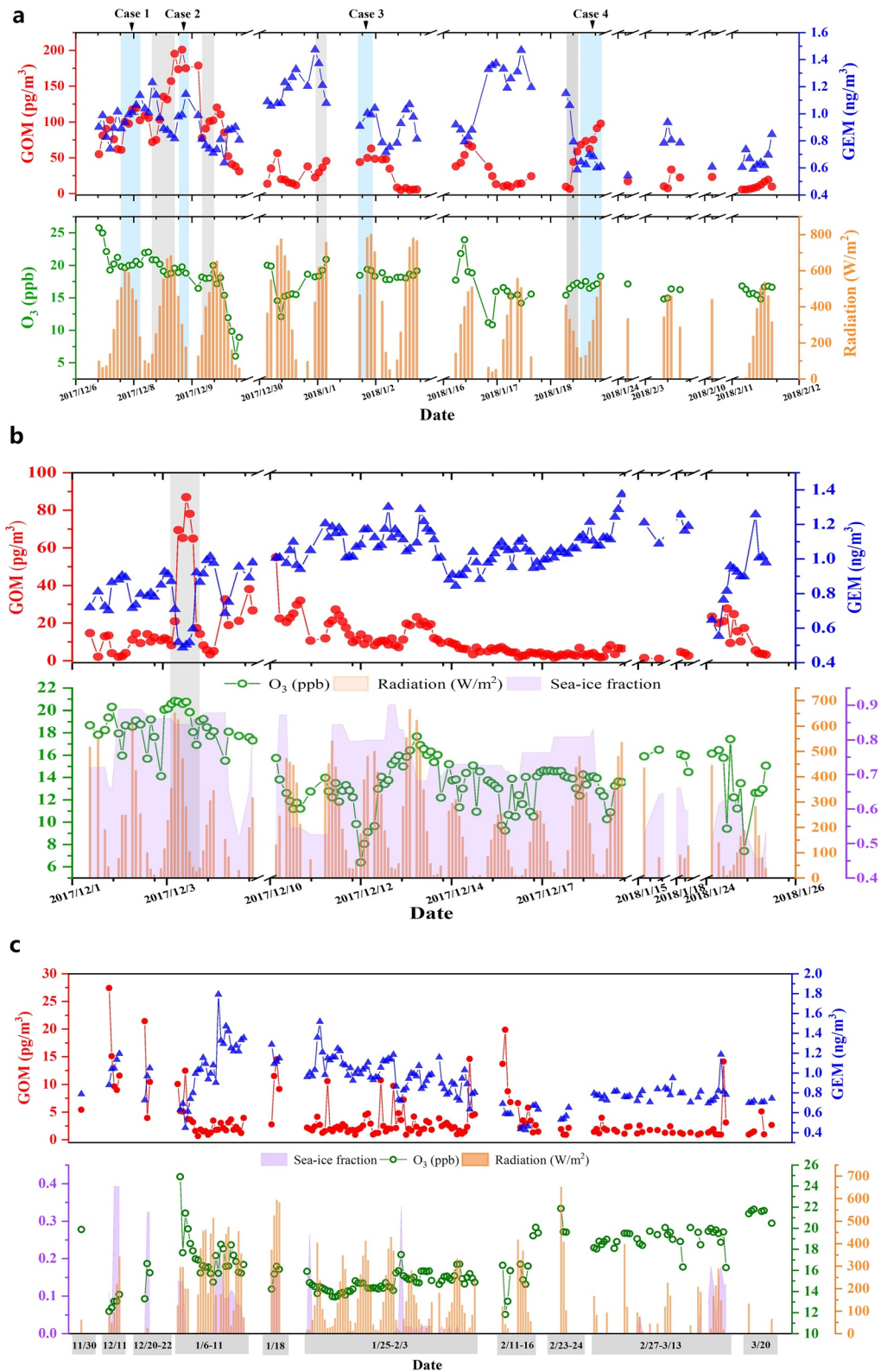


Figure 2. Time series for gaseous oxidized mercury (GOM), 2h-averaged gaseous elemental mercury (GEM), O₃, shortwave radiation, and the sea-ice fraction in (a) coastal Antarctica, (b) the sea-ice region, and (c) the ocean region in this cruise. The gray shaded area shows the periods during which elevations in the GOM were accompanied by synchronous depletions of GEM, and the blue shaded area shows the periods in which elevations in GOM levels were not accompanied by depletions in GEM levels.

the impact of anthropogenic emission on it here. Several evidences indicated that its impact would be negligible for GOM results:

1. As shown in Figure S6, there is no synchronous rising trend or correlation between GEM and NO_x during the whole cruise ($r = 0.0043$) and in Coastal Antarctica ($r = -0.013$), also the same to GOM and NO_x during the whole cruise ($r = 0.065$) and in Coastal Antarctica ($r = 0.071$)
2. The observed GOM concentrations ($<5 \text{ pg/m}^3$) during two berthing periods at Christchurch, New Zealand in this cruise were significantly lower than that in Coastal Antarctica (Figure S7)
3. Laurier et al. (2003) suggested that ship's exhaust gases would lead to contamination with relative wind direction angle (RWD) in the range of 120° – 240° , while statistics showed that 86.3% of the RWD was outside the 120° – 240° range during the whole cruise. We also compared relative wind direction angle with observed GEM and GOM and found no relationship with them. Many periods of elevated concentrations of GEM and GOM corresponded to sparse points of RWD (Figure S8)
4. The concentration levels of GOM measured near Terra Nova Bay (from December 7 to December 10, 2017) in this study are comparable to those measured in McMurdo station by Brooks et al. (2008b) from October 29 to November 4, 2003, which had a similar observed season to this study and were closed to our observation site (in Ross Sea region)

As shown in Figure 2a, parts of the periods in which the increases of GOM concentrations are accompanied by synchronous rapid depletion in GEM concentrations and high values of shortwave radiation (gray shaded area). This indicates the photochemical in-situ oxidation of atmospheric GEM occurred near berthing sites in coastal Antarctica, and the GOM produced here can reach up to 195.37 pg-m^{-3} (the leftmost gray shaded area). Similar results were also observed at Antarctic Terra Nova Bay and Neumayer Station during summertime, with significant elevations in GOM concentrations (up to more than 300 pg-m^{-3} in both cases) accompanied by obvious GEM depletions, indicating a conversion from GEM to GOM (Sprovieri et al., 2002; Temme et al., 2003).

Besides, there were no depletions, even synchronous elevations of GEM concentrations during some periods of elevated GOM concentration (Cases 1–4, blue shaded areas), including the period in which the maximum GOM concentration (201.23 pg-m^{-3}) of this cruise was observed (Figure 2a). We speculated that it may be to some extent related to the local atmospheric physical conditions. In the springtime, the polar troposphere is characterized by stable stratification with weak vertical mixing, and the frequent occurrence of strong surface temperature inversions would inhibit turbulent transport of atmospheric components, which can facilitate the continuous depletion of GEM and O_3 during AMDEs, while the more well mixed troposphere in the polar summertime would not favor the continuous depletion of GEM concentrations during its in-situ oxidation (Nguyen et al., 2009; Steffen et al., 2008). Moreover, it is a unique phenomenon in Antarctica that the negative buoyant force which develops along the ice-sheet slopes will result in strong katabatic winds flowing out from the Antarctic Plateau (Gallée & Pettré, 1998). The observation sites for cases 1–4 are located at Terra Nova Bay, Prydz Bay, and Ross Ice Shelf, respectively (Figure S5a), where the ice-sheet katabatic winds are frequent (Bromwich & Kurtz, 1984; Parish & Bromwich, 2007). The 72 h HYSPLIT backward trajectory results show that the air mass during cases 1–4 came primarily from the Antarctic continent (Figure S9), with a downward velocity originating at high altitudes, which is the typical feature of Antarctic katabatic wind. The katabatic winds would enhance turbulent mixing over this region and facilitate atmospheric transport, which could replenish both GEM and O_3 and caused no depletion during cases 1–4 even if the presence of in-situ oxidation of GEM (Figure 2a).

Furthermore, Brooks et al. (2008a) found that GOM and PBM concentrations observed at the South Pole during summer were positively correlated with the depth of the mixing layer, indicating that oxidized Hg species were entrained from the lower free troposphere and continuously removed via surface deposition at the South Pole. However, in this study, there was no correlation found between GOM and the PBLH (Figure S10). This suggests that the vertical convection input of GOM is minor in coastal Antarctica, which is different from the situation in inland Antarctica.

3.3.3. Sea-Ice Region

The GOM concentrations range from 1.03 to 87.01 pg-m^{-3} in the sea-ice region, which were lower and less variant than in coastal Antarctica (Figure 2b and Table 1). The average concentration of GOM in the sea-ice

region is more than 230% higher than that in the oceanic region (Table 1), which indicates that the existence of sea-ice cover can promote the oxidation of GEM in the Antarctic MBL during the sunlit summer. There was a clear high spike in GOM from December 3 and 4 during the navigation in Ross sea (the gray shaded area in Figure 2b), with the concentrations increasing promptly from 8.23 to 69.50 $\text{pg}\cdot\text{m}^{-3}$ within the first 4 h of that period and finally reaching the maximum at 87.01 $\text{pg}\cdot\text{m}^{-3}$ in the subsequent 4 h. The corresponding 2h-averaged GEM concentrations underwent a significant simultaneous depletion from 0.87 to 0.49 $\text{ng}\cdot\text{m}^{-3}$ and shortwave radiation levels were also high during this period (Figure 2b). These features suggest that significant in-situ photochemical oxidation of GEM can occur in the region of Antarctica that is, covered with sea-ice during summer. Similar to the situation in coastal Antarctica, the 2h-averaged O_3 concentrations corresponding to this period also showed no correlation with GEM, and the chemical mechanisms involved in this process (the oxidation of GEM and/or the production of oxidants) needs further investigation.

As shown in Figure S11, there is a negative logarithmic regression relationship between the GOM levels observed in the sea-ice region and the 2h-averaged GEM level, implying that with the continuous decrease of GEM, the growth rate of GOM (can be expressed as $-\text{dGOM}/\text{dGEM}$, quantified by the absolute value of the tangential slope of the logarithmic fitting of GOM vs. GEM) gradually increased. This result could, to some extent, reflect the low lifetime of GOM in the Antarctic sea-ice region. The more significant depletion of GEM might suggest a shorter time was taken after GEM is oxidized to GOM in the air (otherwise the depletion of GEM would peter out due to the mixing of air mass from other places as time goes by). This is conducive to keeping formed GOM in the air due to its unstable property and results in the logarithmic relationship that it has with GEM, as presented in Figure S11.

Several previous observations have shown that the oxidized atmospheric Hg species in the sea-ice area are mainly in the form of PBM with a low GOM level (M. Nerentorp Mastromonaco et al., 2016; Steffen et al., 2013), which might be attributed to the high particle load of the air. Several laboratory studies have shown that sea salt aerosols have a high capacity to uptake atmospheric GOM (Malcolm et al., 2009; Rutter & Schauer, 2007). Since considerable sea-salt aerosol can be produced by the salt-rich blowing snow and the wave breaking among Antarctic MBL (Han et al., 2017; Lieb-Lappen & Obbard, 2015), synchronous high-resolution field observations of atmospheric Na^+ in aerosol (used in this study as an indicator of sea salt levels) were made during this cruise. Figure 3b shows that GOM is significantly anti-correlated with the 2h-averaged levels of Na^+ in the sea-ice region ($p < 0.01$), implying the uptake effect of sea-salt aerosol on GOM in the sea-ice region. This mechanism was further supported by a similar variation trend between observed Na^+ concentrations and the Hg(II) uptake coefficients of sea-salt aerosol, which was calculated based on the parametric scheme of GEOS-Chem in Holmes et al. (2010) (Figure S12). It might be a non-negligible factor causing GOM loss and the high PBM content in polar sea-ice covered area as observed before, which would then influence its deposition flux. In addition, the concentrations of Na^+ measured in the coastal Antarctica region were generally low (Figure 3a), with a significantly lower average concentration ($107.49 \pm 104.87 \text{ ng}\cdot\text{m}^{-3}$, $n = 173$) than the sea-ice region ($335.03 \pm 428.63 \text{ ng}\cdot\text{m}^{-3}$, $n = 309$), suggesting that the weaker sea salt uptake of GOM could also be a cause of the higher GOM concentrations and GOM/GEM ratios observed in the coastal Antarctica region. The weaker sea salt uptake is also likely, to some extent, to explain the phenomenon of GOM predominating the oxidized atmospheric Hg observed at several inland Antarctic stations, which is opposite to observations from the sea-ice region (Brooks et al., 2008b; Temme et al., 2003).

3.3.4. Oceanic Region

The GOM concentrations observed in the oceanic region during this cruise were the lowest compared to coastal Antarctica and sea-ice regions (Figure 2c and Table 1); the average was similar to the global average ($3.1 \pm 11 \text{ pg}\cdot\text{m}^{-3}$) (Soerensen et al., 2010), and observations in seas in the northern hemispheric (the Mediterranean, Bohai, Yellow, and South China seas and off Okinawa) (Chand et al., 2008; Sprovieri et al., 2003; C. Wang et al., 2016, 2019) (Table S2). Holmes et al. (2009) suggested that 80%–95% of divalent Hg in the MBL was present in sea salt aerosols rather than as a gas phase. The average concentration of Na^+ observed in the oceanic region during this cruise was $875.19 \pm 1,068.61 \text{ ng}\cdot\text{m}^{-3}$ ($n = 165$) and was more than twice that of the sea-ice region and seven times that of coastal Antarctica, suggesting that the high uptake of GOM by sea salt aerosols might be an important factor causing the oceanic region to have the lowest GOM

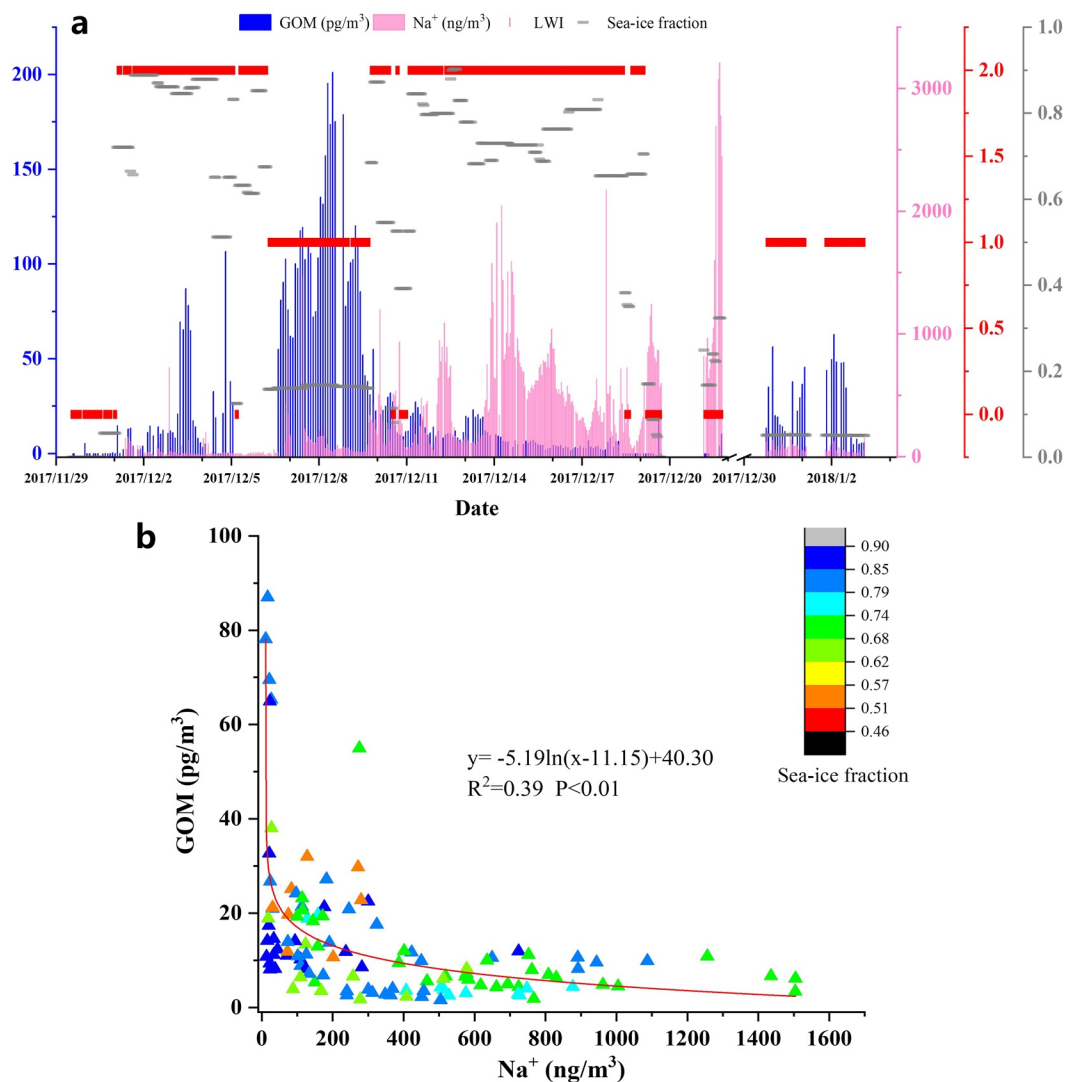


Figure 3. (a) Time-series of measured gaseous oxidized mercury (GOM) levels, atmospheric water-soluble Na⁺ concentrations, and the sea-ice fraction during part of this cruise, which included voyages in coastal Antarctica, the sea-ice region, and the ocean region, and (b) the relationship between the measured GOM levels, the atmospheric Na⁺ concentrations, and the sea-ice fraction during the navigation period in sea-ice region.

level. Our cruise observations in the Ross Sea span from mid-December to late January, featuring obvious sea-ice melting and then caused a majority of the sea-ice region to become the oceanic region based on their respective LWI. As shown in Figure 4e, there are notable differences between the GOM level and GOM/GEM ratios obtained during Cruise 1, which was dominated by the sea-ice region, and Cruise 2, which was oceanic-region dominated although it had a navigation area similar to that of Cruise 1. The average GOM concentrations observed during Cruise 2 ($2.99 \pm 2.22 \text{ pg}\cdot\text{m}^{-3}$) were nearly 85% lower than those from Cruise 1 ($20.15 \pm 4.51 \text{ pg}\cdot\text{m}^{-3}$), along with the apparent melting of the sea-ice between the two cruise periods (Figures 4a–4d). As the first year sea-ice served widely as an important source of active halogen species in the polar region (Luo et al., 2018; Saiz-Lopez et al., 2007; Simpson et al., 2007), sea-ice loss likely weakened the production of active halogens, which slowed GEM oxidation. This is verified by the data from GOME-2 satellite maps that showed an obvious loss in the BrO[•] column concentration for the period between Cruise 1 and Cruise 2 (Figure S13). Our observations suggest that the seasonal melting of the first year sea-ice during summer would decrease the oxidation of GEM, which is also an important factor that causes the low content of GOM in the oceanic region in Antarctica, and might, in turn, change the rate of deposition atmospheric Hg in the Antarctic MBL. In all, the cycle mechanisms of atmospheric mercury in three land

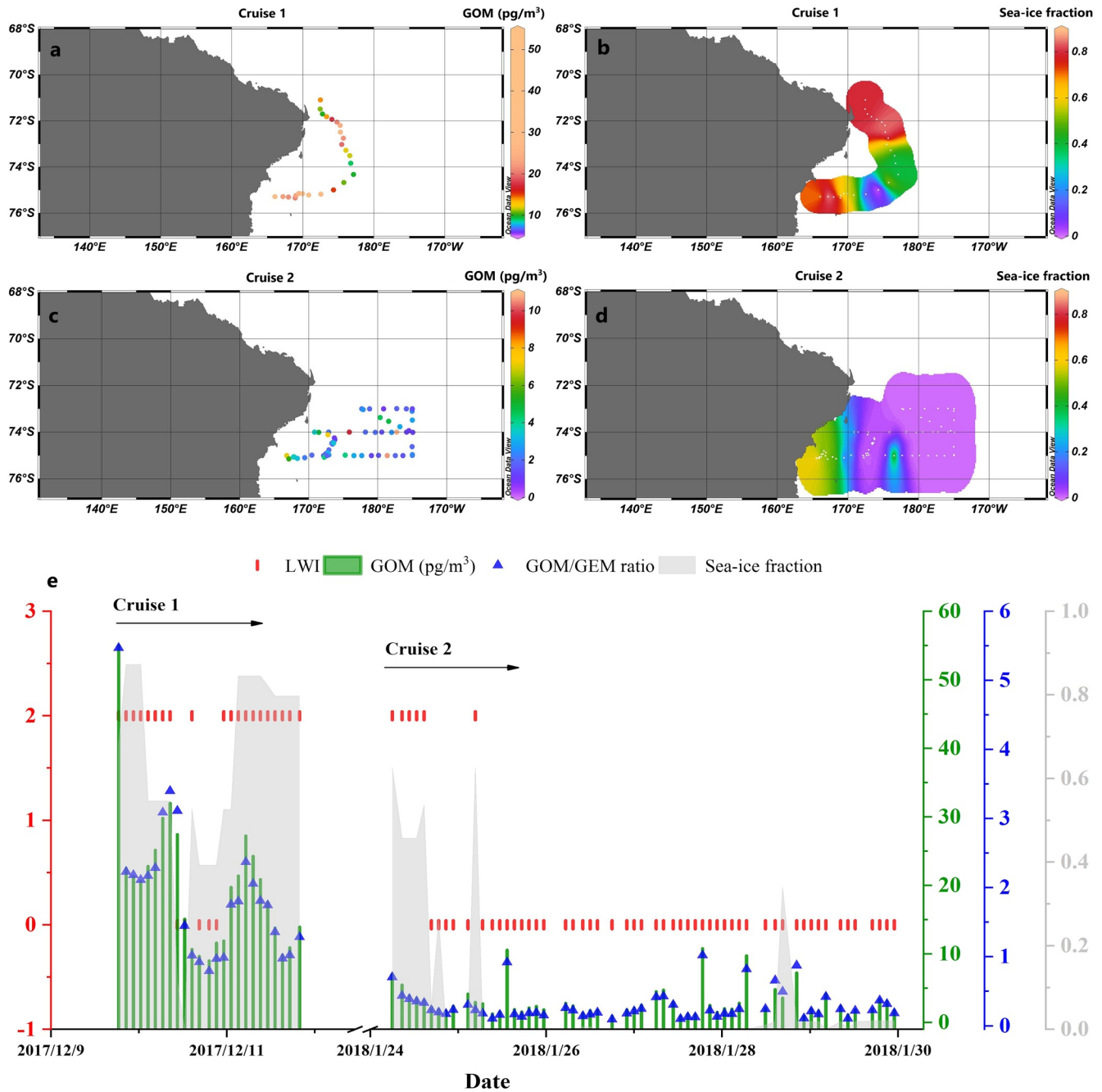


Figure 4. Spatial distributions of gaseous oxidized mercury (GOM) observations and the corresponding sea-ice fraction during Cruise 1 (a and b) and Cruise 2 (c and d). Time-series of GOM concentrations, GOM/ gaseous elemental mercury ratios (%), land–water–ice indices, and sea-ice fractions during Cruise 1 and Cruise 2 in the Ross Sea (e).

surface types among the Southern Ocean in summer, which were discussed in this study, are simply illustrated through a schematic diagram shown in Figure 5.

4. Conclusions

This study reflects that the large discrepancy in the land surface types appears to impact the atmospheric Hg cycle in the Antarctic marine boundary layer, causing large spatial differences in GOM levels. The Antarctic continent can serve as an important source of oxidized Hg during the sunlit summer period, due to

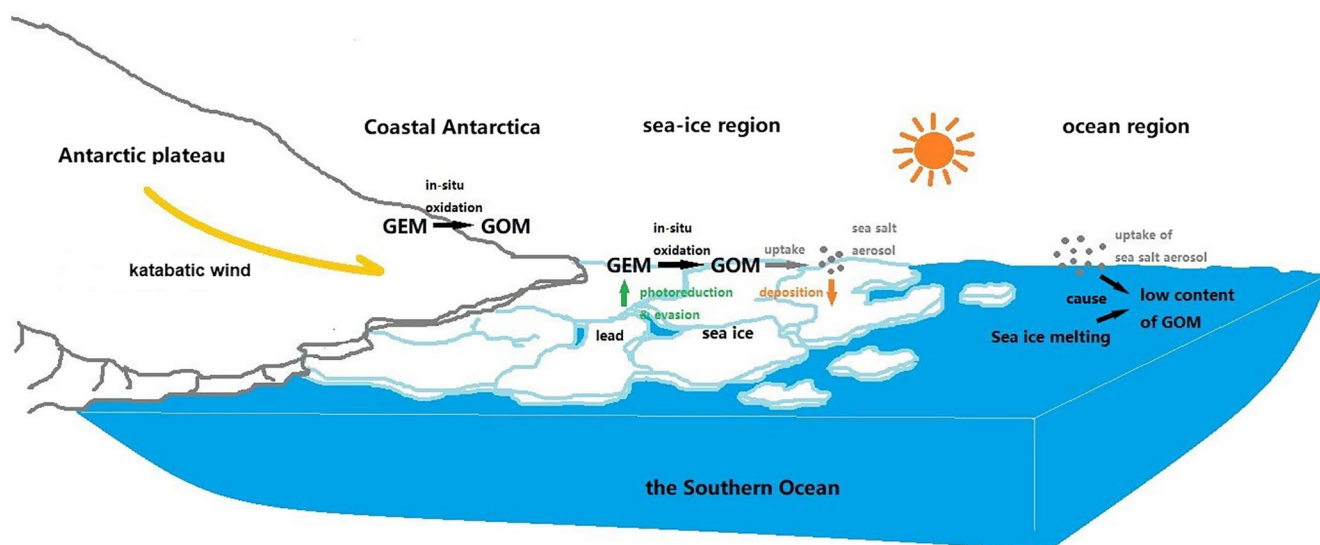


Figure 5. A schematic diagram simply displaying the cycle mechanisms of atmospheric mercury in three land surface types along the Southern Ocean in summer, which were discussed in this study. In coastal Antarctica, the highest gaseous oxidized mercury (GOM) level can be attributed to the in situ oxidation there. In the sea-ice region, the significant in-situ oxidation of gaseous elemental mercury could also occur, while the uptake of the high content of sea-salt aerosols in sea-ice regions might efficiently eliminate GOM in the air. In the oceanic region, the lowest level of GOM is due to both the uptake of sea-salt aerosols and the seasonal melting of first-year sea-ice.

the significant in-situ oxidation there. As coastal Antarctica is a primary habitat for creatures such as penguins, whales, and seals, the ecological effects of their exposure to highly oxidized Hg in this environment are worthy of further attention. In sea-ice regions, the uptake of the high content of sea-salt aerosols might efficiently eliminate atmospheric GOM in the summertime. It would be an important factor that influences the deposition flux of Hg and can explain the phenomenon observed in previous studies that atmospheric oxidized Hg in the sea-ice area mainly takes the form of PBM. In the oceanic region, the lowest level of GOM is attributed to both the uptake of sea-salt aerosols and the seasonal melting of first-year sea ice. In general, our study indicates that the impact of various land surface types should be seriously considered in the estimation of Hg deposition in the Antarctic region, due to their apparently different influencing mechanisms in the atmospheric Hg cycle.

Acknowledgments

This work was supported by the National Natural Science Foundation of China (grant no. 41676173, 41930532), and the Ministry of Natural Resources of the People's Republic of China (IRASCC2020-2022-No.01-01-02E). We thank China Arctic and Antarctic Administration for fieldwork support. We thank Prof. Feiyue Wang at Univ of Manitoba, and Xuewu Fu at the Institute of Geochemistry, Chinese Academy of Sciences for helpful discussion and improving English expression. The authors acknowledge the NOAA Air Resources Laboratory (ARL) for developing the HYSPLIT transport and dispersion model available on the Internet (<https://www.ready.noaa.gov/HYSPLIT.php>).

References

- Andersson, M. E., Sommar, J., Gärdfeldt, K., & Lindqvist, O. (2008). Enhanced concentrations of dissolved gaseous mercury in the surface waters of the Arctic Ocean. *Marine Chemistry*, *110*, 190–194. <https://doi.org/10.1016/j.marchem.2008.04.002>
- Angot, H., Dastoor, A., De Simone, F., Gärdfeldt, K., Gencarelli, C. N., Hedgecock, I. M., et al. (2016). Chemical cycling and deposition of atmospheric mercury in polar regions: Review of recent measurements and comparison with models. *Atmospheric Chemistry and Physics*, *16*, 10735–10763. <https://doi.org/10.5194/acp-16-10735-2016>
- Angot, H., Magand, O., Helmig, D., Ricaud, P., Quennehen, B., Gallée, H., et al. (2016). New insights into the atmospheric mercury cycling in central Antarctica and implications on a continental scale. *Atmospheric Chemistry and Physics*, *16*, 8249–8264. <https://doi.org/10.5194/acp-16-8249-2016>
- Bargagli, R. (2008). Environmental contamination in Antarctic ecosystems. *The Science of the Total Environment*, *400*, 212–226. <https://doi.org/10.1016/j.scitotenv.2008.06.062>
- Brasso, R. L., Polito, M. J., Lynch, H. J., Naveen, R., & Emslie, S. D. (2012). Penguin eggshell membranes reflect homogeneity of mercury in the marine food web surrounding the Antarctic Peninsula. *The Science of the Total Environment*, *439*, 165–171. <https://doi.org/10.1016/j.scitotenv.2012.09.028>
- Bromwich, D. H., & Kurtz, D. D. (1984). Katabatic wind forcing of the Terra Nova Bay polynya. *Journal of Geophysical Research*, *89*, 3561–3572. <https://doi.org/10.1029/JC089iC03p03561>
- Brooks, S., Arimoto, R., Lindberg, S., & Southworth, G. (2008a). Antarctic polar plateau snow surface conversion of deposited oxidized mercury to gaseous elemental mercury with fractional long-term burial. *Atmospheric Environment*, *42*, 2877–2884. <https://doi.org/10.1016/j.atmosenv.2007.05.029>
- Brooks, S., Arimoto, R., Lindberg, S., & Southworth, G. (2008b). Springtime atmospheric mercury speciation in the McMurdo, Antarctica coastal region. *Atmospheric Environment*, *42*, 2885–2893. <https://doi.org/10.1016/j.atmosenv.2007.06.038>
- Carravieri, A., Cherel, Y., Blévin, P., Brault-Favrou, M., Chastel, O., & Bustamante, P. (2014). Mercury exposure in a large subantarctic avian community. *Environmental Pollution*, *190*, 51–57. <https://doi.org/10.1016/j.envpol.2014.03.017>

- Carsey, T. P., Churchill, D. D., Farmer, M. L., Fischer, C. J., Pszenny, A. A., Ross, V. B., et al. (1997). Nitrogen oxides and ozone production in the North Atlantic marine boundary layer. *Journal of Geophysical Research*, *102*, 10653–10665. <https://doi.org/10.1029/96JD03511>
- Chand, D., Jaffe, D., Prestbo, E., Swartzendruber, P. C., Hafner, W., Weiss-Penzias, P., et al. (2008). Reactive and particulate mercury in the Asian marine boundary layer. *Atmospheric Environment*, *42*, 7988–7996. <https://doi.org/10.1016/j.atmosenv.2008.06.048>
- Chaulk, A., Stern, G. A., Armstrong, D., Barber, D. G., & Wang, F. (2011). Mercury distribution and transport across the ocean–sea-ice–atmosphere interface in the Arctic Ocean. *Environmental Science & Technology*, *45*, 1866–1872. <https://doi.org/10.1021/es103434c>
- Cossa, D., Heimbürger, L.-E., Lannuzel, D., Rintoul, S. R., Butler, E. C. V., Bowie, A. R., et al. (2011). Mercury in the Southern Ocean. *Geochimica et Cosmochimica Acta*, *75*, 4037–4052. <https://doi.org/10.1016/j.gca.2011.05.001>
- DiMento, B. P., Mason, R. P., Brooks, S., & Moore, C. (2019). The impact of sea ice on the air-sea exchange of mercury in the Arctic Ocean. *Deep Sea Research Part I: Oceanographic Research Papers*, *144*, 28–38. <https://doi.org/10.1016/j.dsr.2018.12.001>
- Dommergue, A., Sprovieri, F., Pirrone, N., Ebinghaus, R., Brooks, S., Courteau, J., & Ferrari, C. P. (2010). Overview of mercury measurements in the Antarctic troposphere. *Atmospheric Chemistry and Physics*, *10*, 3309–3319. <https://doi.org/10.5194/acp-10-3309-2010>
- Driscoll, C. T., Mason, R. P., Chan, H. M., Jacob, D. J., & Pirrone, N. (2013). Mercury as a global pollutant: Sources, pathways, and effects. *Environmental Science & Technology*, *47*, 4967–4983. <https://doi.org/10.1021/es305071v>
- Durnford, D., & Dastoor, A. (2011). The behavior of mercury in the cryosphere: A review of what we know from observations. *Journal of Geophysical Research*, *116*. <https://doi.org/10.1029/2010jd014809>
- Ebinghaus, R., Kock, H. H., Temme, C., Einax, J. W., Löwe, A. G., Richter, A., et al. (2002). Antarctic springtime depletion of atmospheric mercury. *Environmental Science & Technology*, *36*, 1238–1244. <https://doi.org/10.1021/es015710z>
- Gallée, H., & Pettré, P. (1998). Dynamical constraints on katabatic wind cessation in Adélie Land, Antarctica. *Journal of the Atmospheric Sciences*, *55*, 1755–1770. [https://doi.org/10.1175/1520-0469\(1998\)055<1755:DCOKWC>2.0.CO;2](https://doi.org/10.1175/1520-0469(1998)055<1755:DCOKWC>2.0.CO;2)
- Gay, D. A., Schmeltz, D., Prestbo, E., Olson, M., Sharac, T., & Tordon, R. (2013). The atmospheric mercury network: Measurement and initial examination of an ongoing atmospheric mercury record across North America. *Atmospheric Chemistry and Physics*, *13*, 11339–11349. <https://doi.org/10.5194/acp-13-11339-2013>
- Gustin, M. S., Dunham-Cheatham, S. M., Huang, J. Y., Lindberg, S., & Lyman, S. N. (2021). Development of an understanding of reactive mercury in ambient air: A review. *Atmosphere*, *12*, 73. <https://doi.org/10.3390/atmos12010073>
- Gustin, M. S., Huang, J., Miller, M. B., Peterson, C., Jaffe, D. A., Ambrose, J., et al. (2013). Do we understand what the mercury speciation instruments are actually measuring? Results of RAMIX. *Environmental Science & Technology*, *47*, 7295–7306. <https://doi.org/10.1021/es3039104>
- Han, Y., Huh, Y., Hur, S. D., Hong, S., Chung, J. W., & Motoyama, H. (2017). Net deposition of mercury to the Antarctic Plateau enhanced by sea salt. *The Science of the Total Environment*, *583*, 81–87. <https://doi.org/10.1016/j.scitotenv.2017.01.008>
- Heikes, B., Lee, M., Jacob, D., Talbot, R., Bradshaw, J., Singh, H., et al. (1996). Ozone, hydroperoxides, oxides of nitrogen, and hydrocarbon budgets in the marine boundary layer over the South Atlantic. *Journal of Geophysical Research*, *101*, 24221–24234. <https://doi.org/10.1029/95JD03631>
- Holmes, C. D., Jacob, D. J., Corbitt, E. S., Mao, J., Yang, X., Talbot, R., & Slemr, F. (2010). Global atmospheric model for mercury including oxidation by bromine atoms. *Atmospheric Chemistry and Physics*, *10*, 12037–12057. <https://doi.org/10.5194/acp-10-12037-2010>
- Holmes, C. D., Jacob, D. J., Mason, R. P., & Jaffe, D. A. (2009). Sources and deposition of reactive gaseous mercury in the marine atmosphere. *Atmospheric Environment*, *43*, 2278–2285. <https://doi.org/10.1016/j.atmosenv.2009.01.051>
- Horowitz, H. M., Jacob, D. J., Zhang, Y., Dibble, T. S., Slemr, F., Amos, H. M., et al. (2017). A new mechanism for atmospheric mercury redox chemistry: Implications for the global mercury budget. *Atmospheric Chemistry and Physics*, *17*, 6353–6371. <https://doi.org/10.5194/acp-17-6353-2017>
- Huang, J., & Gustin, M. S. (2015). Uncertainties of gaseous oxidized mercury measurements using KCl-coated denuders, cation-exchange membranes, and nylon membranes: Humidity influences. *Environmental Science & Technology*, *49*, 6102–6108. <https://doi.org/10.1021/acs.est.5b00098>
- Huszar, P., Cariolle, D., Paoli, R., Halenka, T., Belda, M., Schlager, H., et al. (2009). Modeling the regional impact of ship emissions on NOx and ozone levels over the Eastern Atlantic and Western Europe using ship plume parameterization. *Atmospheric Chemistry and Physics Discussions*, *9*, 26735–26776. <https://doi.org/10.5194/acpd-9-26735-2009>
- Lalonde, J. D., Poulain, A. J., & Amyot, M. (2002). The role of mercury redox reactions in snow on snow-to-air mercury transfer. *Environmental Science & Technology*, *36*, 174–178. <https://doi.org/10.1021/es010786g>
- Landis, M. S., Stevens, R. K., Schaedlich, F., & Prestbo, E. M. (2002). Development and characterization of an annular denuder methodology for the measurement of divalent inorganic reactive gaseous mercury in ambient air. *Environmental Science & Technology*, *36*, 3000–3009. <https://doi.org/10.1021/es015887t>
- Laurier, F. J. G., Mason, R. P., Whalin, L., & Kato, S. (2003). Reactive gaseous mercury formation in the North Pacific Ocean's marine boundary layer: A potential role of halogen chemistry. *Journal of Geophysical Research*, *108*. <https://doi.org/10.1029/2003JD003625>
- Li, C., Chen, J., Angot, H., Zheng, W., Shi, G., Ding, M., et al. (2020). Seasonal variation of mercury and its isotopes in atmospheric particles at the coastal Zhongshan Station, Eastern Antarctica. *Environmental Science & Technology*, *54*(18), 11344–11355. <https://doi.org/10.1021/acs.est.0c04462>
- Lieb-Lappen, R. M., & Obbard, R. W. (2015). The role of blowing snow in the activation of bromine over first-year Antarctic sea ice. *Atmospheric Chemistry and Physics*, *15*, 7537–7545. <https://doi.org/10.5194/acp-15-7537-2015>
- Lindberg, S. E., Brooks, S., Lin, C. J., Scott, K. J., Landis, M. S., Stevens, R. K., et al. (2002). Dynamic oxidation of gaseous mercury in the Arctic troposphere at polar sunrise. *Environmental Science & Technology*, *36*, 1245–1256. <https://doi.org/10.1021/es0111941>
- Luo, Y., Si, F., Zhou, H., Dou, K., Liu, Y., & Liu, W. (2018). Observations and source investigations of the boundary layer bromine monoxide (BrO) in the Ny-Ålesund Arctic. *Atmospheric Chemistry and Physics*, *18*, 9789–9801. <https://doi.org/10.5194/acp-18-9789-2018>
- Malcolm, E. G., Ford, A. C., Redding, T. A., Richardson, M. C., Strain, B. M., & Tetzner, S. W. (2009). Experimental investigation of the scavenging of gaseous mercury by sea salt aerosol. *Journal of Atmospheric Chemistry*, *63*, 221–234. <https://doi.org/10.1007/s10874-010-9165-y>
- Marusczak, N., Sonke, J. E., Fu, X., & Jiskra, M. (2017). Tropospheric GOM at the Pic du Midi Observatory—Correcting bias in denuder based observations. *Environmental Science & Technology*, *51*, 863–869. <https://doi.org/10.1021/acs.est.6b04999>
- McClure, C. D., Jaffe, D. A., & Edgerton, E. S. (2014). Evaluation of the KCl denuder method for gaseous oxidized mercury using HgBr2 at an in-service AMNet site. *Environmental Science & Technology*, *48*, 11437–11444. <https://doi.org/10.1021/es502545k>
- McElroy, C. T., McLinden, C. A., & McConnell, J. C. (1999). Evidence for bromine monoxide in the free troposphere during the Arctic polar sunrise. *Nature*, *397*, 338–341. <https://doi.org/10.1038/16904>
- Moore, C. W., Obrist, D., Steffen, A., Staebler, R. M., Douglas, T. A., Richter, A., & Nghiem, S. V. (2014). Convective forcing of mercury and ozone in the Arctic boundary layer induced by leads in sea ice. *Nature*, *506*, 81–84. <https://doi.org/10.1038/nature12924>

- Nerentorp Mastromonaco, M., Gärdfeldt, K., Jourdain, B., Abrahamsson, K., Granfors, A., Ahnoff, M., et al. (2016). Antarctic winter mercury and ozone depletion events over sea ice. *Atmospheric Environment*, 129, 125–132. <https://doi.org/10.1016/j.atmosenv.2016.01.023>
- Nerentorp Mastromonaco, M. G., Gärdfeldt, K., Assmann, K. M., Langer, S., Delali, T., Shlyapnikov, Y. M., et al. (2017). Speciation of mercury in the waters of the Weddell, Amundsen and Ross Seas (Southern Ocean). *Marine Chemistry*, 193, 20–33. <https://doi.org/10.1016/j.marchem.2017.03.001>
- Nerentorp Mastromonaco, M. G., Gärdfeldt, K., & Langer, S. (2017). Mercury flux over West Antarctic Seas during winter, spring and summer. *Marine Chemistry*, 193, 44–54. <https://doi.org/10.1016/j.marchem.2016.08.005>
- Nerentorp Mastromonaco, M. G., Gärdfeldt, K., Langer, S., & Dommergue, A. (2016). Seasonal study of mercury species in the Antarctic sea ice environment. *Environmental Science & Technology*, 50, 12705–12712. <https://doi.org/10.1021/acs.est.6b02700>
- Nguyen, H. T., Kim, K.-H., Shon, Z.-H., & Hong, S. (2009). A review of atmospheric mercury in the polar environment. *Critical Reviews in Environmental Science and Technology*, 39, 552–584. <https://doi.org/10.1080/10643380701764308>
- Parish, T. R., & Bromwich, D. H. (2007). Reexamination of the near-surface airflow over the Antarctic continent and implications on atmospheric circulations at high southern latitudes. *Monthly Weather Review*, 135, 1961–1973. <https://doi.org/10.1175/MWR3374.1>
- Radke, L. F., Friedli, H. R., & Heikes, B. G. (2007). Atmospheric mercury over the NE Pacific during spring 2002: Gradients, residence time, upper troposphere lower stratosphere loss, and long-range transport. *Journal of Geophysical Research*, 112. <https://doi.org/10.1029/2005JD005828>
- Rutter, A. P., & Schauer, J. J. (2007). The impact of aerosol composition on the particle to gas partitioning of reactive mercury. *Environmental Science & Technology*, 41, 3934–3939. <https://doi.org/10.1021/es062439i>
- Saiz-Lopez, A., Mahajan, A. S., Salmon, R. A., Bauguitte, S. J. B., Jones, A. E., Roscoe, H. K., & Plane, J. M. C. (2007). Boundary layer halogens in Coastal Antarctica. *Science*, 317, 348–351. <https://doi.org/10.1126/science.1141408>
- Schroeder, W. H., Anlauf, K. G., Barrie, L. A., Lu, J. Y., Steffen, A., Schneeberger, D. R., & Berg, T. (1998). Arctic springtime depletion of mercury. *Nature*, 394, 331–332. <https://doi.org/10.1038/28530>
- Simpson, W. R., Carlson, D., Hönninger, G., Douglas, T. A., Sturm, M., Perovich, D., & Platt, U. (2007). First-year sea-ice contact predicts bromine monoxide (BrO) levels at Barrow, Alaska better than potential frost flower contact. *Atmospheric Chemistry and Physics*, 7, 621–627. <https://doi.org/10.5194/acp-7-621-2007>
- Soerensen, A. L., Skov, H., Jacob, D. J., Soerensen, B. T., & Johnson, M. S. (2010). Global concentrations of gaseous elemental mercury and reactive gaseous mercury in the marine boundary layer. *Environmental Science & Technology*, 44, 7425–7430. <https://doi.org/10.1021/es903839n>
- Sprovieri, F., Pirrone, N., Bencardino, M., D'Amore, F., Carbone, F., Cinnirella, S., et al. (2016). Atmospheric mercury concentrations observed at ground-based monitoring sites globally distributed in the framework of the GMOS network. *Atmospheric Chemistry and Physics*, 16, 11915–11935. <https://doi.org/10.5194/acp-16-11915-2016>
- Sprovieri, F., Pirrone, N., Gärdfeldt, K., & Sommar, J. (2003). Mercury speciation in the marine boundary layer along a 6000km cruise path around the Mediterranean Sea. *Atmospheric Environment*, 37, 63–71. [https://doi.org/10.1016/S1352-2310\(03\)00237-1](https://doi.org/10.1016/S1352-2310(03)00237-1)
- Sprovieri, F., Pirrone, N., Hedgecock, I. M., Landis, M. S., & Stevens, R. K. (2002). Intensive atmospheric mercury measurements at Terra Nova Bay in Antarctica during November and December 2000. *Journal of Geophysical Research*, 107, ACH 20-21–ACH 20-28. <https://doi.org/10.1029/2002JD002057>
- Steffen, A., Bottenheim, J., Cole, A., Douglas, T. A., Ebinghaus, R., Friess, U., et al. (2013). Atmospheric mercury over sea ice during the OASIS-2009 campaign. *Atmospheric Chemistry and Physics*, 13, 7007–7021. <https://doi.org/10.5194/acp-13-7007-2013>
- Steffen, A., Douglas, T., Amyot, M., Ariya, P., Aspö, K., Berg, T., et al. (2008). A synthesis of atmospheric mercury depletion event chemistry in the atmosphere and snow. *Atmospheric Chemistry and Physics*, 8, 1445–1482. <https://doi.org/10.5194/acp-8-1445-2008>
- Steffen, A., Lehnert, I., Cole, A., Ariya, P., Dastoor, A., Durnford, D., et al. (2015). Atmospheric mercury in the Canadian Arctic. Part I: A review of recent field measurements. *The Science of the Total Environment*, 509–510, 3–15. <https://doi.org/10.1016/j.scitotenv.2014.10.109>
- Steve, L., Russell, B., Ralf, E., Daniel, E., Xinbin, F., & William, F. (2007). A synthesis of progress and uncertainties in attributing the sources of mercury in deposition. *AMBIO: A Journal of the Human Environment*, 36, 19–33. [https://doi.org/10.1579/0044-7447\(2007\)36\[62:tmdomp\]2.0.co;2](https://doi.org/10.1579/0044-7447(2007)36[62:tmdomp]2.0.co;2)
- Temme, C., Einax, J. W., Ebinghaus, R., & Schroeder, W. H. (2003). Measurements of atmospheric mercury species at a coastal site in the Antarctic and over the South Atlantic Ocean during polar summer. *Environmental Science & Technology*, 37, 22–31. <https://doi.org/10.1021/es025884w>
- Vinken, G. C. M., Boersma, K. F., van Donkelaar, A., & Zhang, L. (2014). Constraints on ship NO_x emissions in Europe using GEOS-Chem and OMI satellite NO₂ observations. *Atmospheric Chemistry and Physics*, 14, 1353–1369. <https://doi.org/10.5194/acp-14-1353-2014>
- Wang, C., Ci, Z., Wang, Z., Zhang, X., & Guo, J. (2016). Speciated atmospheric mercury in the marine boundary layer of the Bohai Sea and Yellow Sea. *Atmospheric Environment*, 131, 360–370. <https://doi.org/10.1016/j.atmosenv.2016.02.021>
- Wang, C., Wang, Z., Hui, F., & Zhang, X. (2019). Speciated atmospheric mercury and sea–air exchange of gaseous mercury in the South China Sea. *Atmospheric Chemistry and Physics*, 19, 10111–10127. <https://doi.org/10.5194/acp-19-10111-2019>
- Wang, F., Saiz-Lopez, A., Mahajan, A. S., Gómez Martín, J. C., Armstrong, D., Lemes, M., et al. (2014). Enhanced production of oxidised mercury over the tropical Pacific Ocean: A key missing oxidation pathway. *Atmospheric Chemistry and Physics*, 14, 1323–1335. <https://doi.org/10.5194/acp-14-1323-2014>
- Wang, J., Xie, Z., Wang, F., & Kang, H. (2017). Gaseous elemental mercury in the marine boundary layer and air–sea flux in the Southern Ocean in austral summer. *The Science of the Total Environment*, 603–604, 510–518. <https://doi.org/10.1016/j.scitotenv.2017.06.120>
- Wang, J., Zhang, L., & Xie, Z. (2016). Total gaseous mercury along a transect from coastal to central Antarctic: Spatial and diurnal variations. *Journal of Hazardous Materials*, 317, 362–372. <https://doi.org/10.1016/j.jhazmat.2016.05.068>
- Wang, S., McNamara, S. M., Moore, C. W., Obrist, D., Steffen, A., Shepson, P. B., et al. (2019). Direct detection of atmospheric atomic bromine leading to mercury and ozone depletion. *Proceedings of the National Academy of Sciences*, 116, 14479–14484. <https://doi.org/10.1073/pnas.1900613116>
- Xia, C., Xie, Z., & Sun, L. (2010). Atmospheric mercury in the marine boundary layer along a cruise path from Shanghai, China to Prydz Bay, Antarctica. *Atmospheric Environment*, 44, 1815–1821. <https://doi.org/10.1016/j.atmosenv.2009.12.039>
- Xie, Z. Q., Sander, R., Pöschl, U., & Slemr, F. (2008). Simulation of atmospheric mercury depletion events (AMDEs) during polar springtime using the MECCA box model. *Atmospheric Chemistry and Physics*, 8, 7165–7180. <https://doi.org/10.5194/acp-8-7165-2008>
- Yan, J., Jung, J., Zhang, M., Bianchi, F., Tham, Y. J., Xu, S., et al. (2020). Uptake selectivity of methanesulfonic acid (MSA) on fine particles over polynya regions of the Ross Sea, Antarctica. *Atmospheric Chemistry and Physics*, 20, 3259–3271. <https://doi.org/10.5194/acp-20-3259-2020>